Available online at www.sciencedirect.com
SCIENCE DIRECT®
Journal of Power Sources 138 (2004) 145–155
JOURNAL OF POWER SOURCES
www.elsevier.com/locate/jpowsour

Curvature in solid oxide fuel cells

Wenxia Li[a,*], Kathy Hasinska[b], Matt Seabaugh[b], Scott Swartz[b], John Lannutti[a,*]

[a] *Department of Materials Science and Engineering, The Ohio State University, 2041 College Rd., Columbus, OH 43210, USA*
[b] *NexTech Materials Ltd., 404 Enterprise Dr., Lewis Center, OH 43035, USA*

Received 27 May 2004; accepted 21 June 2004
Available online 17 August 2004

Abstract

At this point in history, curvature is inherent to the laminated components that comprise solid oxide fuel cells (SOFCs). Surprisingly, however, this fact has never been previously quantified in the literature. In addition, potential curvature changes associated with NiO reduction and re-oxidation during operation have not been investigated. In this report, an optical profilometer was employed to non-destructively quantify the surface curvature or cracking behavior observed on a large scale in industrially manufactured cells. This provides insights into the challenges that the component materials face as well as additional appreciation for why, in spite of a concerted effort to commercialize SOFC power generation, all currently manufactured SOFC stacks fail. Our results demonstrate that cracked electrolyte areas (caused by differential sintering) are flatter than uncracked regions. The height of the electrolyte surface ranged from 86 to 289 μm above the baseline following sintering. Reduction typically results in increases in curvature of up to 214 μm. Initial crack density appears to affect curvature evolution during reduction; the higher the crack density, the smaller the curvature increase following reduction at 600 °C. In general, however, we observed that the electrolyte layer is remarkably resistant to further cracking during these typographic changes. Following oxidation at 750 °C, large changes in curvature (up to 280 μm) are noted that appear to be related to the strength of the bond between the electrolyte and the underlying anode.

Keywords: Warpage; Glassy seals; Leakage; Electrochemical; Hydrogen

1. Introduction

A variety of stresses exist in solid oxide fuel cell stacks [1–4]. Stresses inherent to each cell may be caused by (1) differential sintering [4–6]; (2) mismatches in thermal expansion between the electrolyte, anode and cathode layers [7] during operation; (3) applied assembly stresses exacerbated by curvature originating during tape casting and lamination and (4) stresses resulting from electrochemical operation, such as those due to thermal cycling or NiO reduction/reoxidation.

These stresses can lead to substantial differences in dimensional change either between or in each individual cell within a stack. Any mismatched dimensional response to heating during stack manufacturing or operation could lead to loss of stack integrity. For a given individual cell, such stresses could result in cracking of the electrolyte and subsequent failure of the cell and other cells around it.

Historically, those cracks typically observed in these multilayered composites are (1) channel cracking caused by tensile stresses due to mismatched thermal expansion coefficients that develop during sintering [8,9]; (2) so-called 'mud' cracks originating from differential drying or sintering within individual layers [8]; (3) layer delamination [2,9] and (4) edge-effect cracking and delamination caused by compressive stresses [8,9]. Cracks originating from differential drying and sintering processes appear to result in larger crack displacements than those originating from simple thermal mismatch [8,9]. Either SEM or optical microscopy [8–10] is usually used to detect and observe the behavior of these cracks. However, these two methods usually require destructive sample preparation. In addition, observing crack distributions across the entire surface of a single cell via SEM can be very time consuming as this technique only

* Corresponding authors. Tel.: +1 614 292 3926; fax: +1 614 292 1537.
E-mail addresses: li.448@osu.edu (W. Li), lannutti.1@osu.edu (J. Lannutti).

0378-7753/$ – see front matter © 2004 Elsevier B.V. All rights reserved.
doi:10.1016/j.jpowsour.2004.06.034

examines a relatively small area (around 2.5 mm × 3 mm) even at its lowest magnifications.

The availability of non-destructive methods to characterize curvature or cracking behavior on a larger scale have thus become important in addressing long-standing "show stoppers" in the push to commercialize SOFC power generation. In this paper, an optical surface profilometer was employed to detect crack density distributions in the electrolyte layer of individual, industrially manufactured SOFCs. In addition, since the profilometer measures specimen surface height, scanning the surface of a cracked specimen before and after relevant heat treatments was used to examine the possible linkage between either curvature change or cracking and the corresponding chemical stresses anticipated during long term operation.

2. Experimental procedure

Gadolinia stabilized ceria containing 10 mol% of gadolinia (GDC) and nickel oxide (NiO) were co-mixed at the 50 vol.% Ni (m) level, tape cast and laser cut into circles 1 in. (25.4 mm) in diameter (NexTech Materials Ltd., Lewis Center, OH). These circles were laminated at 80 °C and 2000 psi (14 MPa) to form anode substrates. By heating at 1 °C/min to 600 °C, these substrates were burned out at 600 °C and then heated to 1250 °C for 1 h (at 5 °C/min) to provide sufficient strength for handling. The lightly sintered substrates were then spray coated with a GDC electrolyte layer using an aerosol spray deposition process. The resulting samples were air dried and then sintered at either 1350 or 1400 °C for 1 h, respectively, utilizing a heating rate of 2 °C/min. The samples were sintered in groups of five, sandwiched between two 10 cm × 10 cm × 500 μm thick porous ceria-coated YSZ plates. The GDC electrolytes of one 1400 °C (labeled as 'A') and two 1350 °C sintered specimens ('B' and 'C') were examined using a non-contact surface profilometer (Wyko NT 3300, Veeco Metrology Group, Tucson, AZ) following these sintering steps. R_z, the distance between the average of the top 10 peaks and the average of the bottom 10 valleys, was calculated to provide a quantitative estimate of the overall surface variation. For a more microstructural comparison, the specimens were carbon-coated and specific areas of the electrolyte surface were observed under SEM (XL-30 ESEM-FEG, Philips). In all cases we carefully monitored exactly the same area of the specimen following each thermal treatment.

To evaluate the effect of NiO reduction during operation of the fuel cell on curvature and cracking, these same specimens were reduced at 400 °C for 2 h and at 600 °C for 24 h, respectively, using a 5% H_2–N_2 atmosphere. To observe the effects of oxidation on curvature, these specimens were then oxidized in air at 750 °C for 24 h. To confirm that reduction and oxidation were completed, the weight loss of three similar anode discs (25.4 mm in diameter) were measured following identical reduction and oxidation steps, respectively.

3. Results

3.1. Crack density versus sintering temperature

Fig. 1 shows electrolyte surface images obtained from the optical profilometer. The overall surface variation (R_z = 289) of specimen A sintered at 1400 °C is much larger than that of the specimens sintered at 1350 °C (R_z = 102 and 86 μm for B and C, respectively). A key observation relevant to all cells examined to date is that even though specimens B and C are produced using exactly the same process, the curvature of each specimen is unique.

To better reveal smaller-scale surface features, the images shown in Fig. 2 are processed to remove the spherical surface curvature. Once this is done, a variety of cracks and crack sizes become clearly visible. Specimen A exhibits the highest crack density, specimen C the lowest. Images taken at higher magnifications on certain areas of the specimens (Fig. 3) indicate that the specimen sintered at higher temperature generates a complete network of cracks, while the specimens sintered at the lower temperature tend to display a more scattered array. In addition, the profilometry consistently shows that the crack edges are raised up relative to the surrounding surface. As observed during measurement of curvature, B and C display clear differences in both the pattern and density of cracking.

3.2. Crack density distribution versus position

To better understand the relationship of curvature behavior or residual stress and crack distribution, the crack density in the coating surface was estimated by magnifying the profilometry surface data. The results are schematically shown in Fig. 4. Twelve-color maps were employed to better illustrate the surface curvature of each specimen. Paradoxically, this showed that wherever the surface appears to be the flattest corresponds to the location of the highest crack densities.

3.3. Comparison of profilometry and SEM

SEM was performed to provide higher resolution observations of crack morphology in comparison to the results of profilometry. Fig. 5(a) and (b) shows a direct comparison of cracked and uncracked areas of the electrolyte. Consistency is apparent between the two techniques. While the profilometer cannot detect or distinguish very small, micron-level cracks (see Fig. 5(c)) it does clearly image the surrounding raised up areas and relate them to localized changes in curvature.

3.4. Surface curvature post-reduction and oxidation

The weight loss behavior (Fig. 6) of the three specimens shows that reduction is nearly complete at 600 °C. Following reduction, the surface morphology was examined using both profilometry and SEM (Fig. 5(a) and Fig. 7(a) and (b)). Even using the higher resolutions inherent to SEM, no obvious

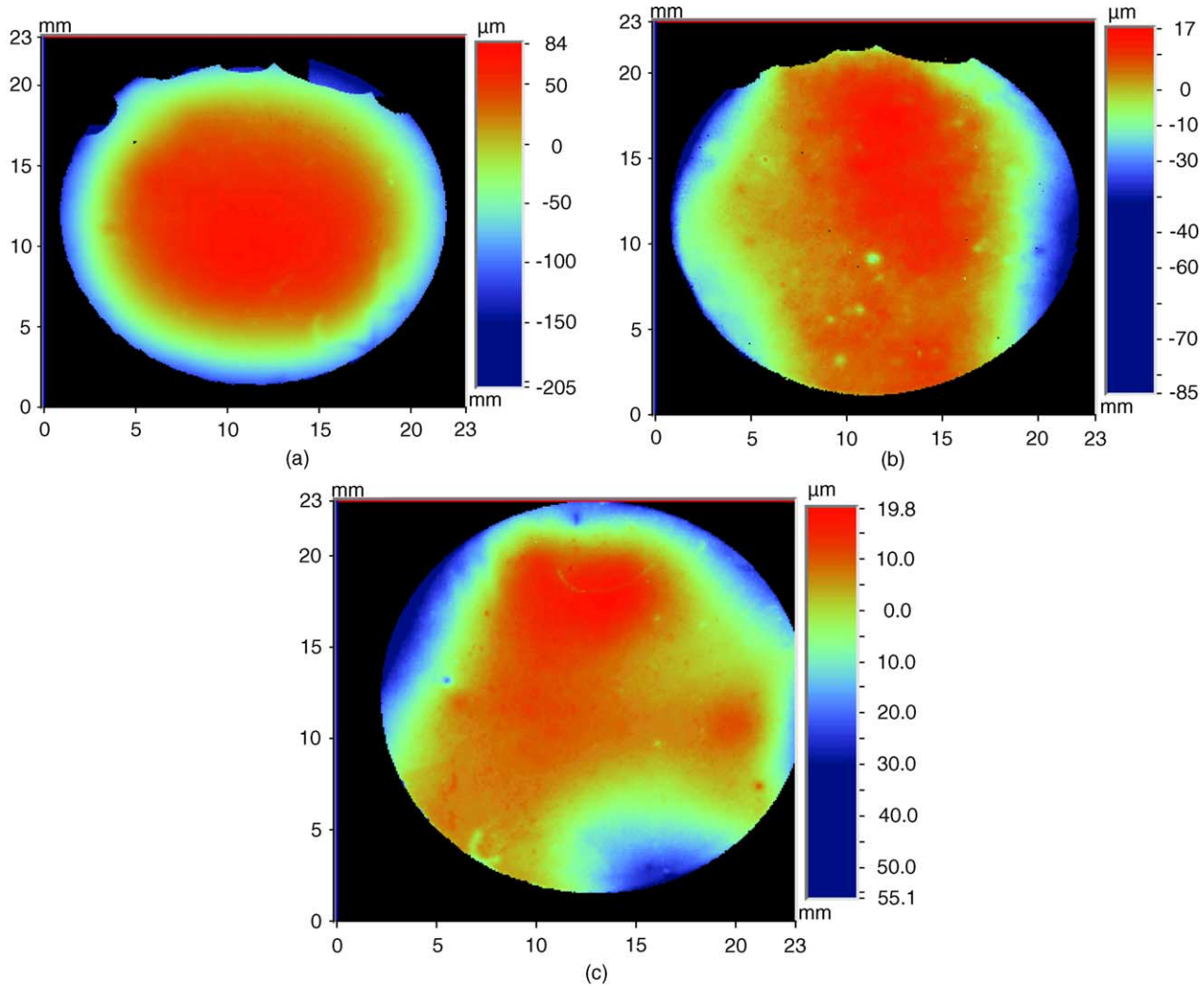

Fig. 1. Profilometry images of specimens sintered at various temperatures: (a) specimen A sintered at 1400 °C, (b) specimen B sintered at 1350 °C and (c) specimen C sintered at 1350 °C. The color bar provides a scale revealing the variation in surface height.

microstructural changes are observed (compare Fig. 5(c) and Fig. 7(c)) except that the surface in the upper right-hand side of Fig. 7(c) appears to be higher. However, profilometry shows that reduction increases the overall surface variation by approximately 30–40 μm for A and B and 200 μm for C (Fig. 8). The plots generated following reduction at 400 and 600 °C also indicate that the overall curvature increases are initiated at the edge of these specimens.

Following the rapid oxidation of these reduced specimens, the overall curvature of samples A and B increased by approximately 280 and 200 μm, respectively, while that of specimen C remained almost unchanged. Again, Fig. 6 shows that the three anode specimens were fully oxidized following exposure to 750 °C. Profilometry shows that the localized curvature near the edge of the specimen increases (Fig. 9). Delamination of the anode layers was observed in those edges close to the electrolyte layers showing the greatest damage (Fig. 2). In some cases, SEM shows that this abrupt curvature change resulted in a greater density of new cracks in the electrolyte layer (Fig. 10).

4. Discussion

4.1. Overall surface curvature, crack density and residual stress

During densification, these specimens curved toward the anode substrate even while under constraint. The overall surface variation increased as the sintering temperature increased (Fig. 1, color bar). Mismatched sintering shrinkage of the different layers provides a potential explanation. The electrolyte layer reaches full density while the anode layers are still quite porous. The higher the sintering temperature, the greater the shrinkage experienced by the anode layers and, therefore, the greater shrinkage differences generated between the anode and the already dense electrolyte. Compressive stresses generated in the electrolyte can then lead to cracking. Lower sintering temperatures apparently resulted in smaller shrinkage differences and lower crack densities. Once the overall curvature is subtracted from the profilometry images, the crack densities in the electrolyte layers can

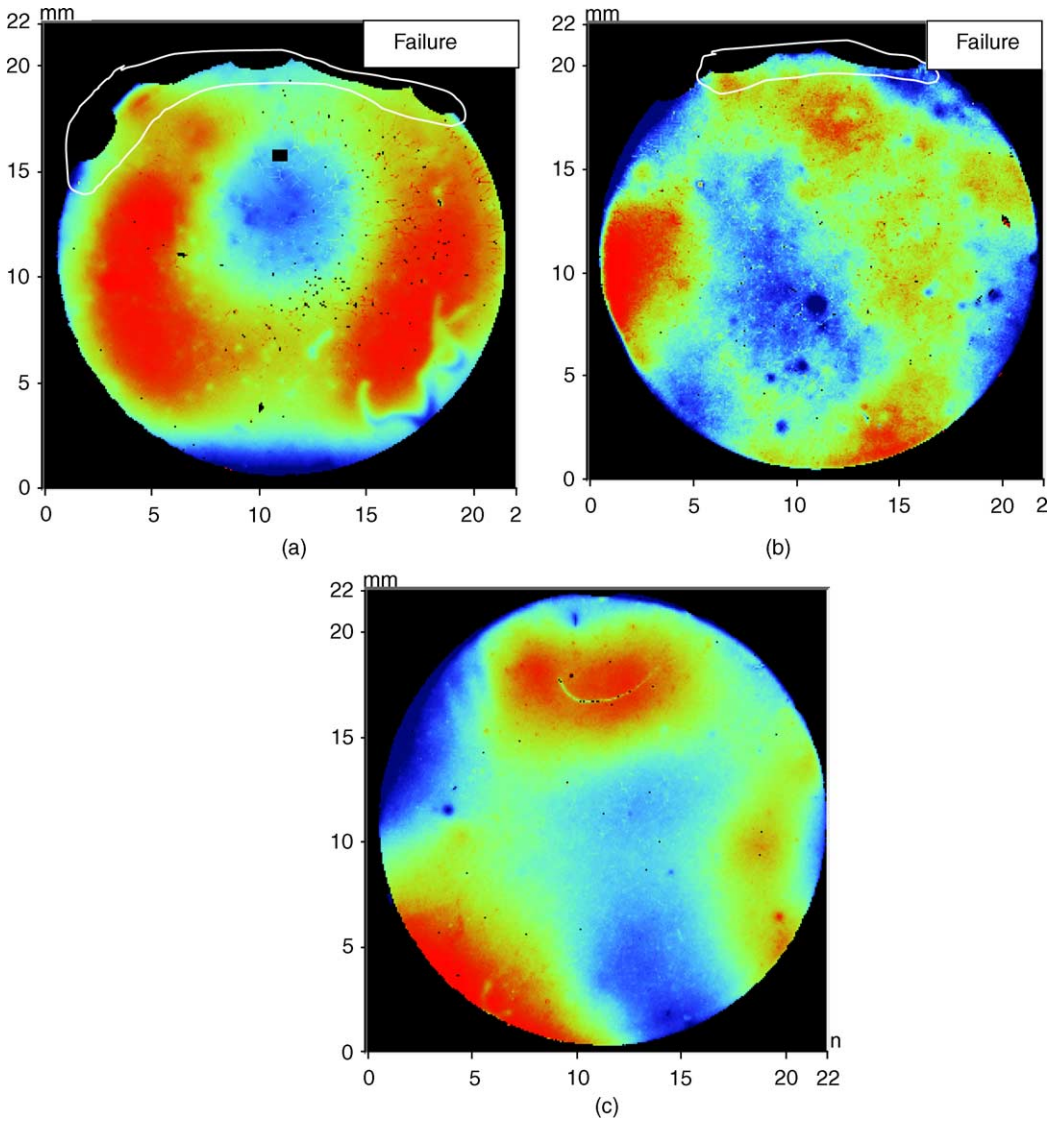

Fig. 2. Profilometry images with curvature removed taken from specimens (a) A, (b) B and (c) C. The failures in the electrolyte coating are indicated.

be clearly resolved. The higher the sintering temperature, the greater the shrinkage differences between the two components and, therefore, a greater incidence of network cracks were observed in the electrolyte coating (Figs. 2 and 3).

In general, the curvature of a dense electrolyte of a multilayer composite specimen should be a combination of prior manufacturing and current residual stresses. Larger curvatures likely reflect a larger residual stress. Once the residual stress in the electrolyte layer goes above a critical level, cracks occur and stress is released [10]. In Fig. 4, the areas in which the surface height changes rapidly appear to have either a low crack density or no cracks at all. This suggests that high residual mismatch stresses are concentrated around those areas. In the cracked areas, this same mismatch stress is released by cracking and the residual stress (if any) is small and this produces the relatively flat areas shown in the color maps of Fig. 4. In addition, the constraint on top of the specimen during sintering likely contributes both to the flatness (via gravimetric constraint) and to cracking (via frictional constraint). These areas are those in which manufacturing stresses leading to curvature were concentrated and contacted the constraining surface with the greatest force.

The overall surface curvature increased during reduction as shown in Fig. 8. All specimens curved even more toward the anode layer (see Fig. 8) probably due to the additional shrinkage generated by the reduction of the NiO to Ni [11]. This indicates that reduction must produce at least some stresses within the specimen. Because little or no constraint exists at the edges of the specimen, these free edges tend to deform preferentially to release the shrinkage stresses caused by reduction. Surprisingly, both SEM and profilometry failed to reveal any significant microstructural-level damage resulting from these large macroscopic changes even in the presence of very sharp cracks (Fig. 7). This demonstrates that the electrolyte layer has far more compliance than was previously anticipated. The quantitative data from profilometry

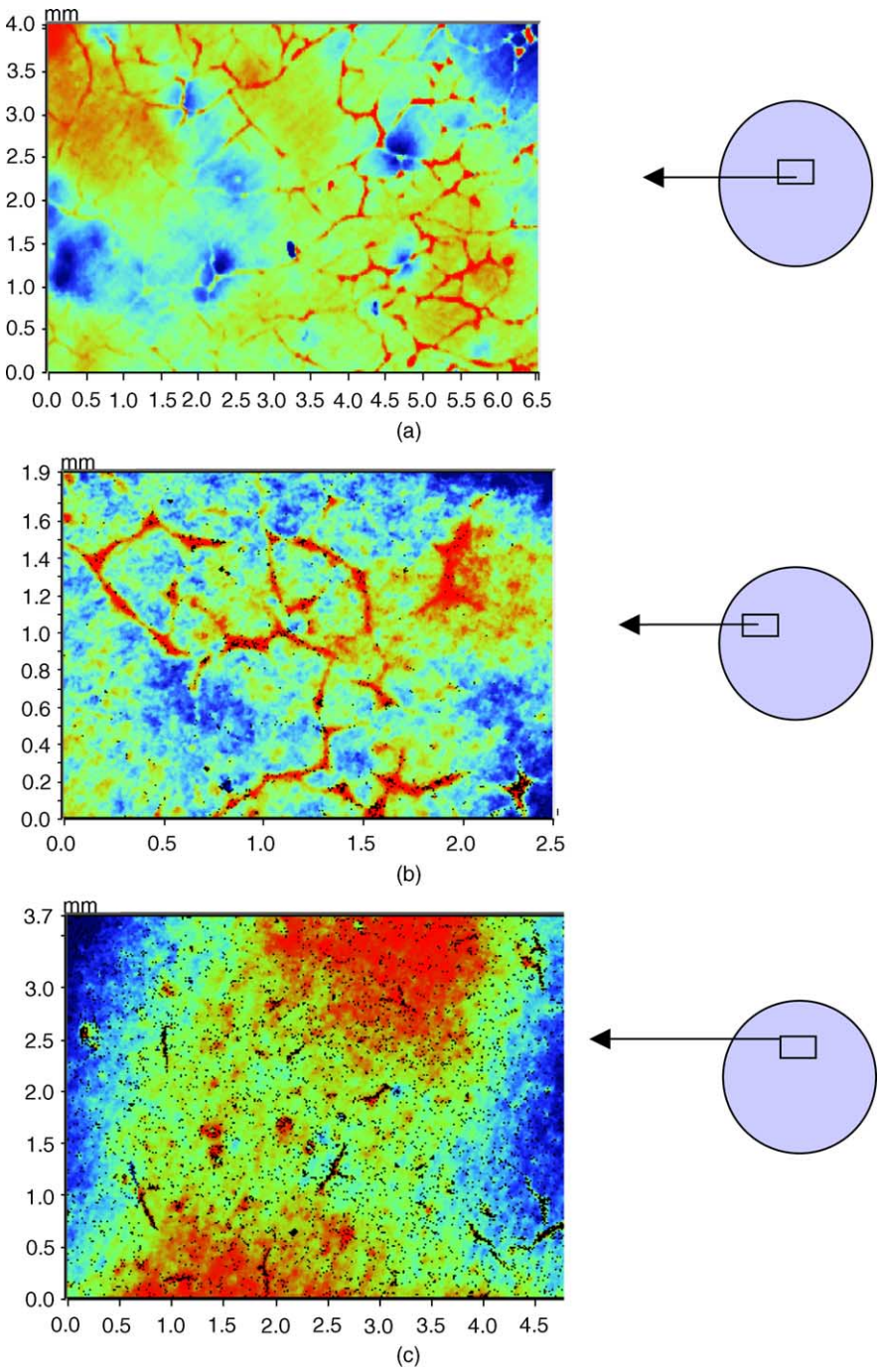

Fig. 3. Profilometry images of selected areas from specimens (a) A, (b) B and (c) C. The schematics show the location of the selected areas in the corresponding specimen.

(Fig. 8) was able to reveal the overall curvature changes, an additional advantage of the surface profilometer as a manufacturing diagnostic tool.

4.2. Crack types and morphology via profilometry

By comparing the initial morphology of the cracks in the electrolyte layer with those found in the non-fuel cell literature [8,9], we can conclude that both larger cracks due to sintering or cosintering mismatches (Fig. 5(a) and (c)) and fine 'channeling' cracks due to thermal mismatch (Fig. 5(c)) were detected. Profilometry can obviously detect cracks that have substantially larger crack separations. It also shows that the edges of these cracks are elevated above the surrounding electrolyte consistent with the fact that this coating experiences compressive stress resulting from non-optimal shrinkage of the anode layer. Although SEM can detect finer cracks, profilometry can provide statistically valid information

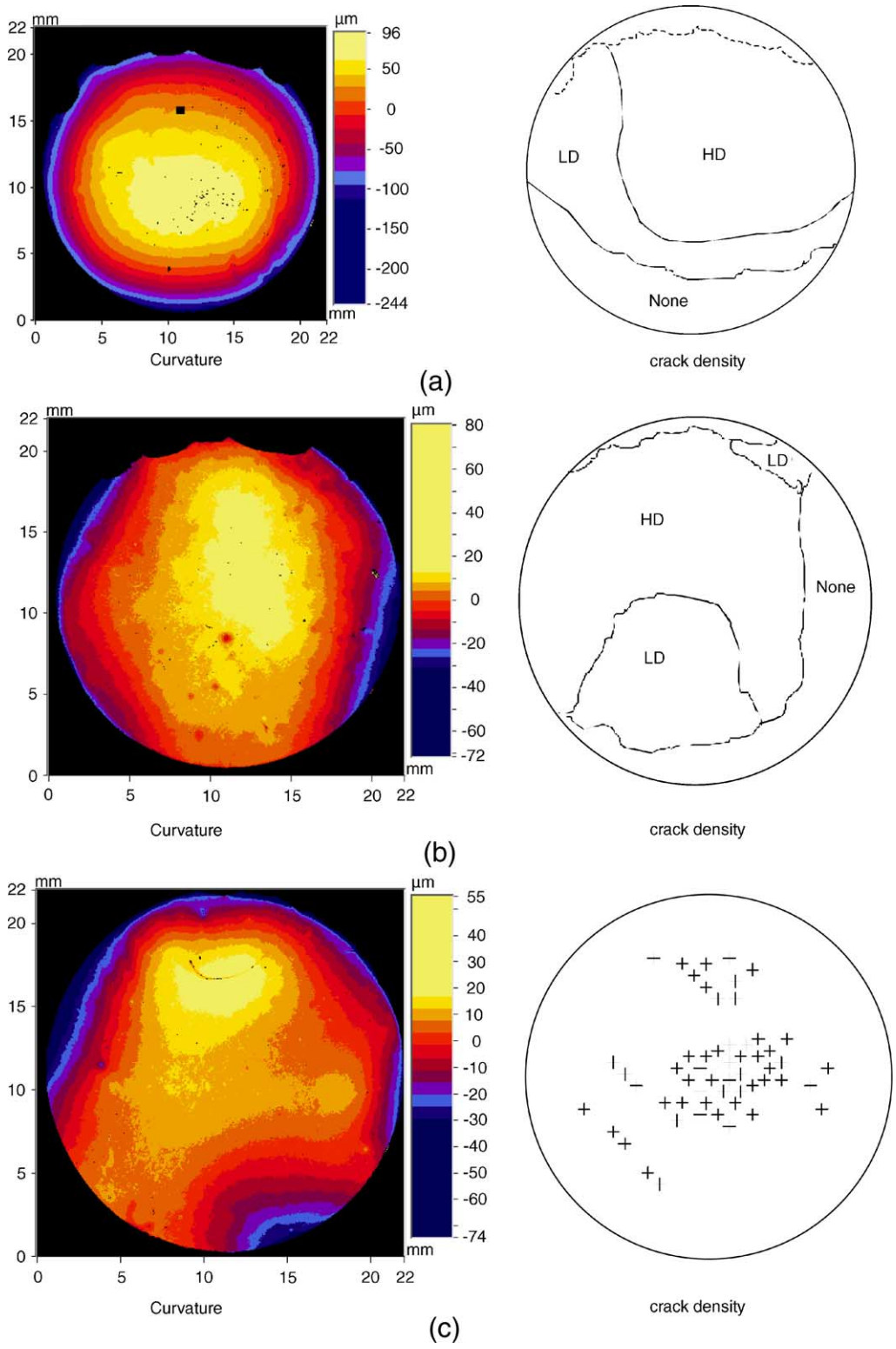

Fig. 4. Curvature vs. crack density in the coating of specimens (a) A, (b) B and (c) C. HD: high crack density, LD: low crack density, none: no cracking, +: crack.

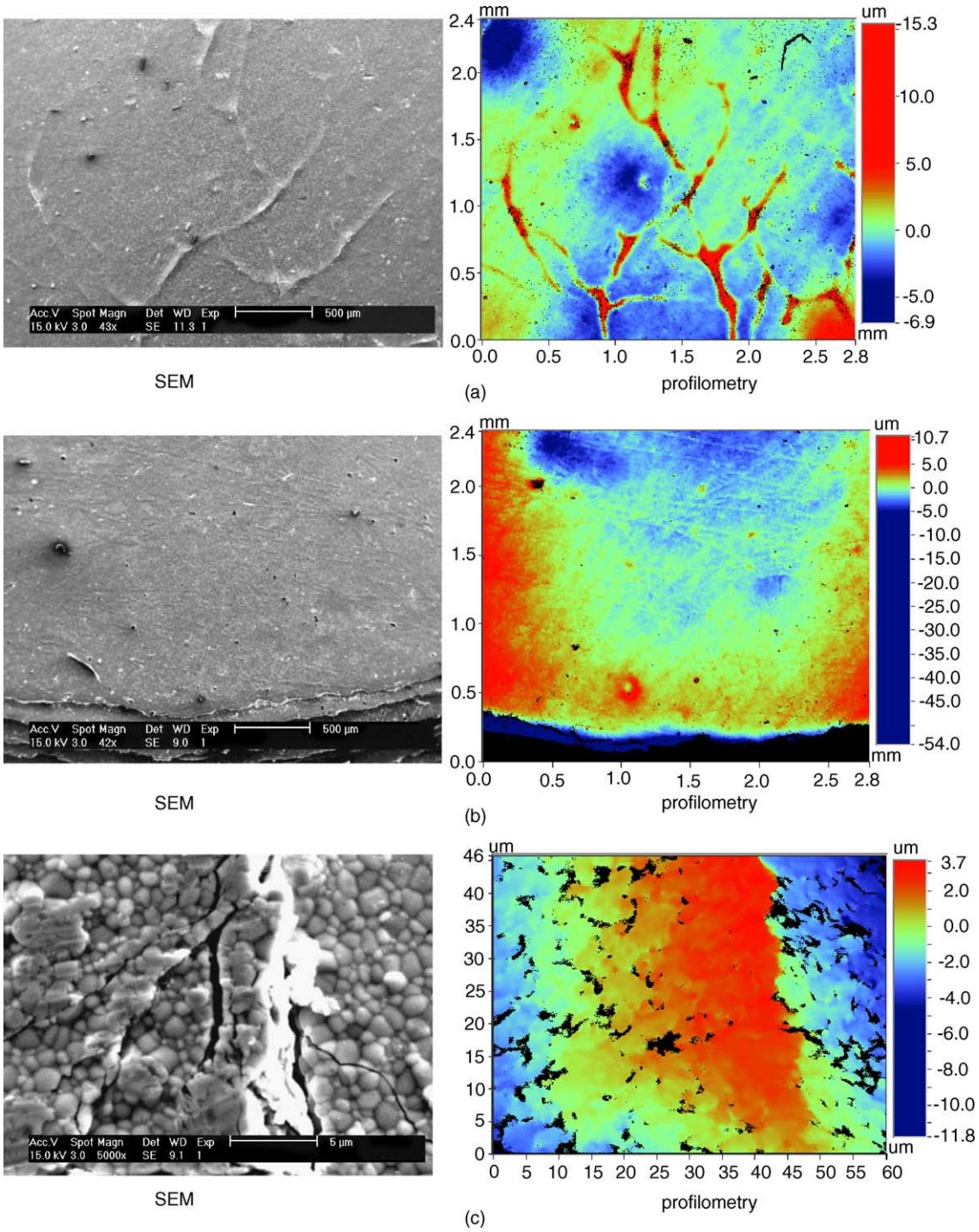

Fig. 5. Comparison between SEM and profilometry of the cracked coating surface in the as-sintered specimens: (a) cracked area, (b) uncracked area and (c) small cracks.

(distribution, morphology and location) regarding the large cracks likely to lead to mechanical and electrochemical failure in a completely non-destructive manner.

4.3. Crack density and curvature

Interestingly, following reduction the curvature of specimens A and B are similar (Fig. 8(a) and (b)) even though they were sintered at different temperatures. The curvature evolution of specimen C is markedly different from that of A and B, especially following reduction at 600 °C. Crack density in the electrolyte following sintering may be responsible. Figs. 2 and 3 clearly show that cracks in the electrolyte surfaces of A and B are part of a crack network while those in C are more widely scattered. In addition, the crack densities in A and B are much higher than in C. Therefore, it is reasonable

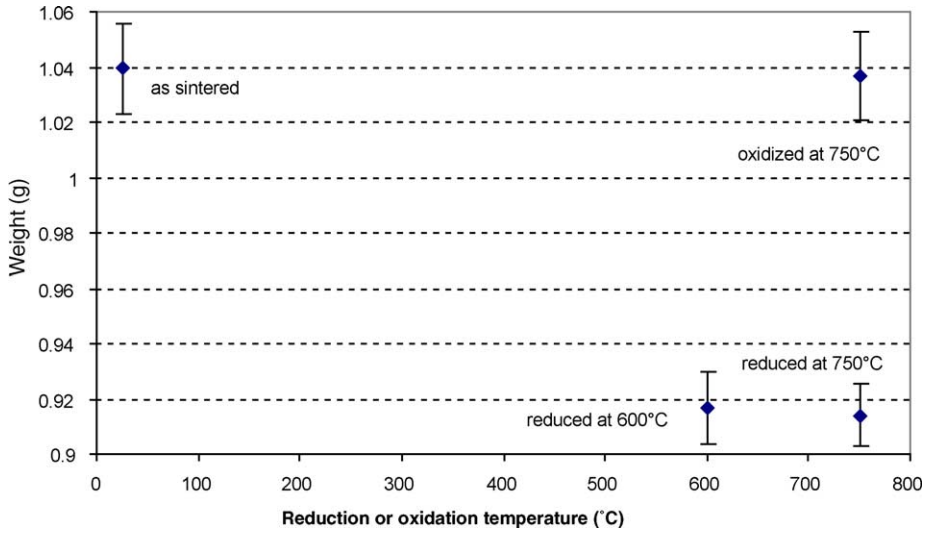

Fig. 6. Gravimetric behavior of anode specimens following reduction at 600, 750 and oxidation at 750 °C, respectively.

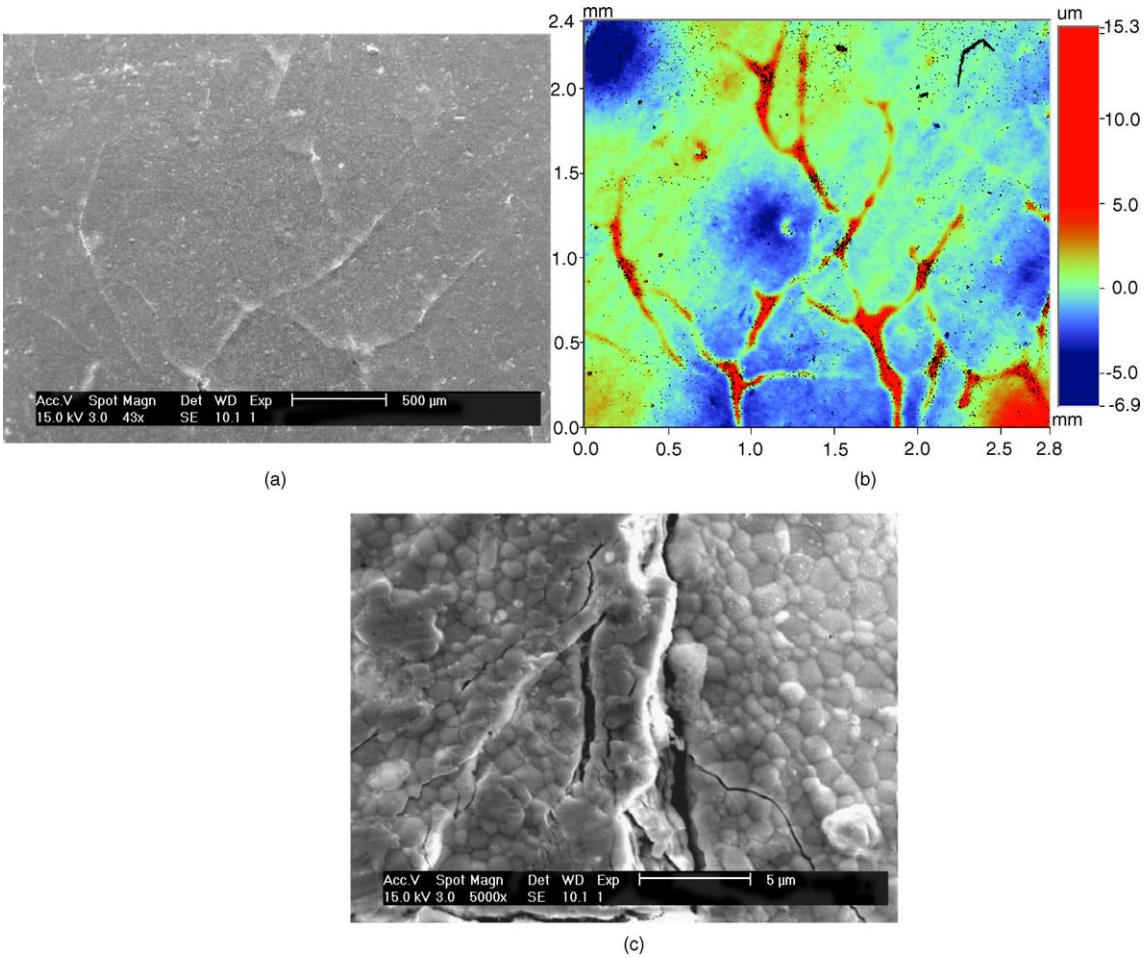

Fig. 7. Comparison of surface morphology between SEM and profilometry post-reduction at 600 °C: (a) SEM and (b) profilometric morphologies of the same zone in Fig. 5(a) after reduction and (c) SEM of the same zone in Fig. 5(c).

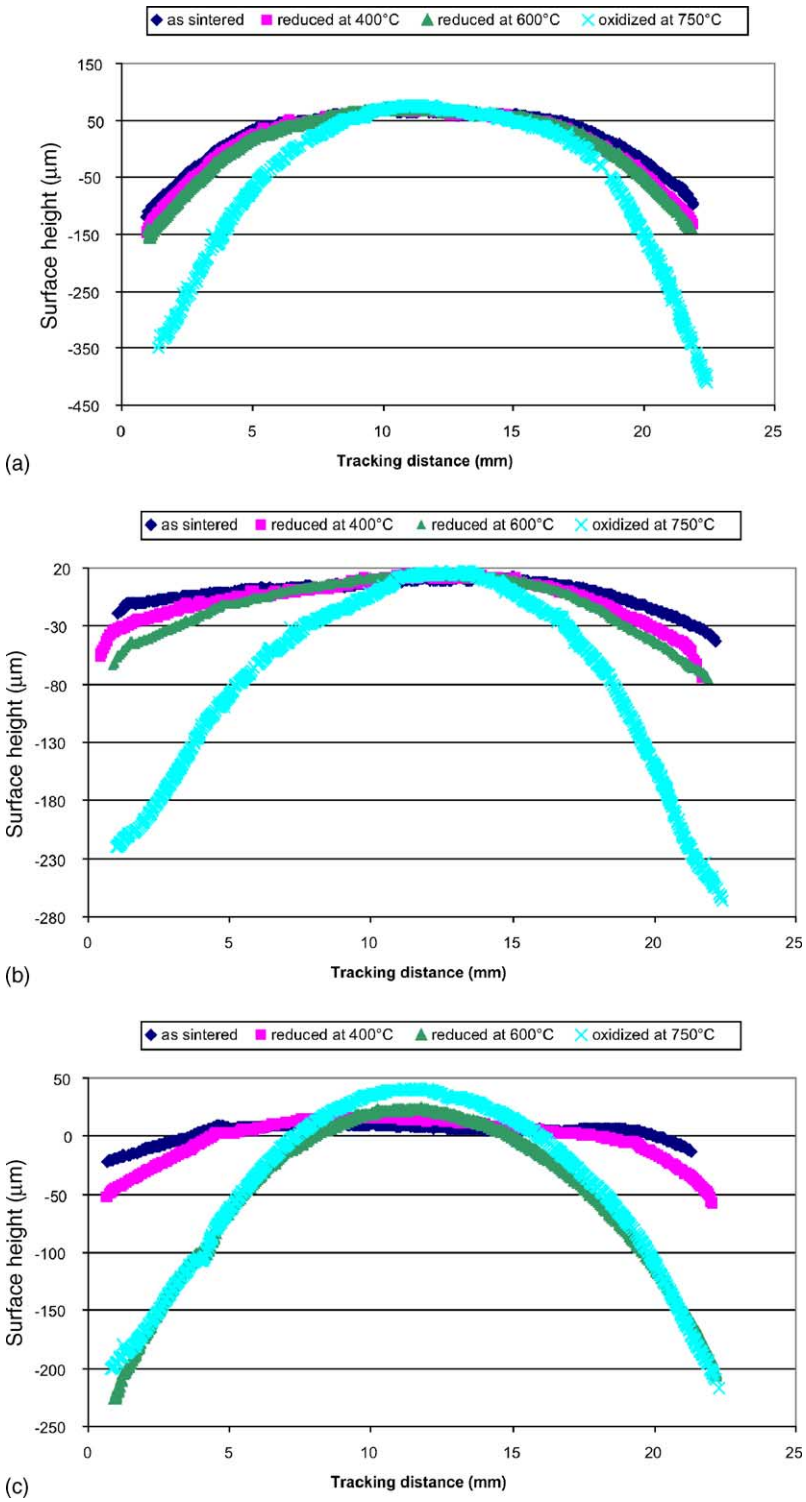

Fig. 8. Comparison of curvature along same diameter before and after reduction/oxidation for specimens (a) A, (b) B and (c) C.

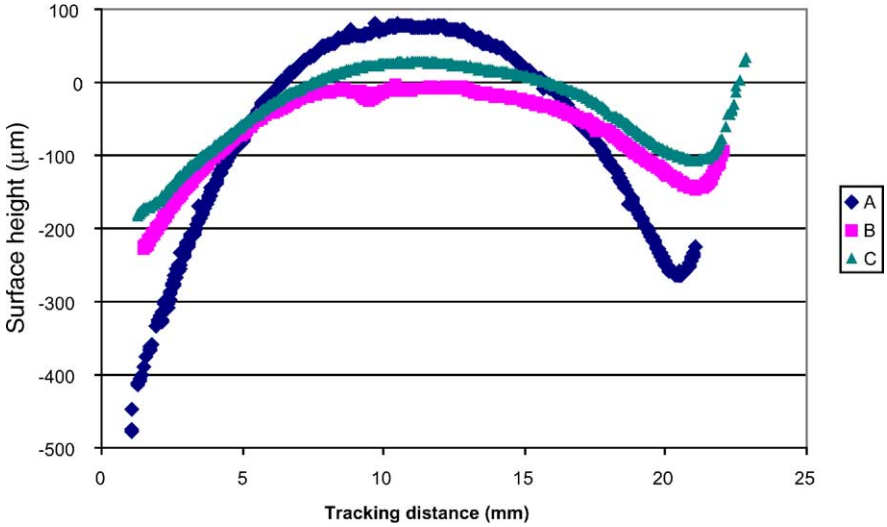

Fig. 9. Curvature in specimen A–C across the center following oxidation at 750 °C.

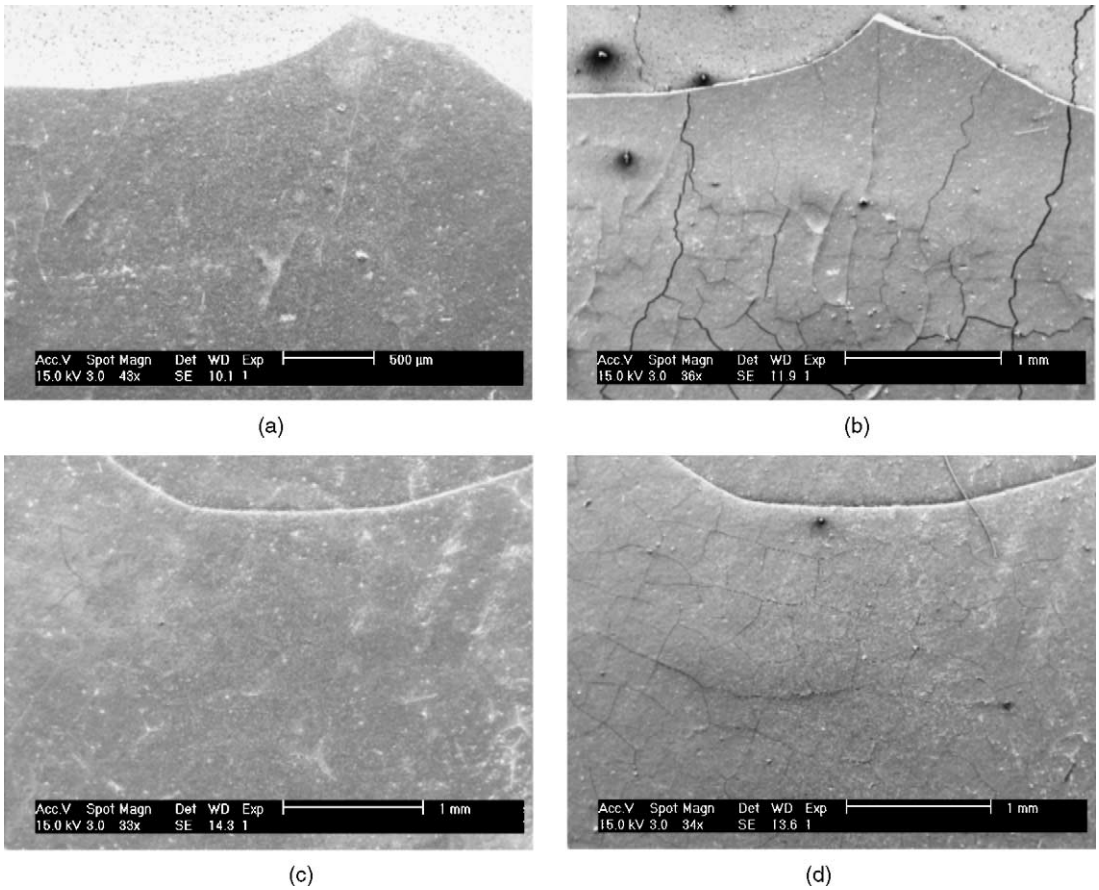

Fig. 10. SEM surface morphology before and after oxidation at 750 °C: (a) specimen A post-reduction at 600 °C, (b) same area in (a) post-oxidation, (c) specimen C post-reduction at 600 °C and (d) same area in (c) post-oxidation. New channeling cracks developed in both the electrolyte and the anode.

to infer that the interfacial strength between the electrolyte and the anode substrate in specimen C was stronger than that in specimens A and B. The constraint of the electrolyte layer by the substrate in A and B would be much smaller than that in C when the substrate shrank due to the reduction of NiO to Ni. This likely resulted in smaller increases in curvature following reduction at 600 °C.

The most dramatic consequence of this becomes obvious following the rapid oxidation of the reduced specimens: the curvature of samples A and B increased substantially while that of C remained almost unchanged. This is contrary to the commonly accepted idea that oxidation causes expansion in the anode substrate [11] and should reverse the curvature observed following reduction. This phenomenon is probably due to the combined effects of both delamination and oxidation. The delamination in specimen C is likely contained within the anode due to the stronger bonding between the electrolyte and the top layer of the anode. In addition, the oxidative expansion was released by the electrolyte cracking and, therefore, specimen C exhibits little visible change in curvature following oxidation (Fig. 8(c)). On the other hand, the electrolyte–substrate bonding of specimen A is weaker. Following oxidation the effects of the delamination in the anode substrate can transfer to the top surface and lead to significant surface curvature change (Fig. 8(a)). In addition, non-uniform oxidation in these laminates could also conceivably contribute to the curvature changes [12]. Carefully designed experiments are needed to further test this hypothesis.

5. Conclusions

Non-contact profilometry can detect sintering cracks non-destructively and provide quantitative data regarding curvature changes before and after sintering, reduction and reoxidation. The cracked areas of the electrolyte initiated by differential sintering are flatter than uncracked regions. NiO reduction results in increases in curvature. Initial crack density affects curvature evolution during reduction; the higher the crack density, the smaller the curvature increase following reduction at 600 °C.

References

[1] R.K. Bordia, R. Raj, J. Am. Ceram. Soc. 68 (1985) 287–292.
[2] A.G. Evans, J.W. Hutchinson, Acta Metall. Mater. 43 (1995) 2507–2530.
[3] C. Hillman, Z. Suo, F.F. Lange, J. Am. Ceram. Soc. 79 (1996) 2127–2133.
[4] H. Tomaszewski, H. Weglarz, M. Boniecki, W.M. Recko, J. Mater. Sci. 35 (2000) 4165–4176.
[5] R. Okuyama, E. Nomura, J. Ceram. Soc. Jpn. 101 (1993) 1001–1005.
[6] T. Garino, Ceram. Eng. Sci. Proc. 23 (2002) 759–765.
[7] S. Majumdar, T. Claar, B. Flandermeyer, J. Am. Ceram. Soc. 69 (1986) 628–633.
[8] B.F. Sørensen, S. Primdahl, J. Mater. Sci. 33 (1998) 5291–5300.
[9] P.Z. Cai, D.J. Green, G.L. Messing, J. Am. Ceram. Soc. 80 (1997) 1929–1939.
[10] A. Selcuk, G. Merere, A. Atkinson, J. Mater. Sci. 36 (2001) 1173–1182.
[11] M. Mori, T. Yamamoto, H. Itoh, H. Inaba, H. Tagawa, J. Electrochem. Soc. 145 (1998) 1374–1381.
[12] G. Stathis, D. Simwonis, F. Tietz, A. Moropoulou, A. Naoumides, J. Mater. Res. 17 (2002) 951–958.